Int J Adv Manuf Technol (2014) 72:1625–1637
DOI 10.1007/s00170-014-5774-y

ORIGINAL ARTICLE

Investigations on the automatic precision polishing of curved surfaces using a five-axis machining centre

Deyang Feng · Yuwen Sun · Huapeng Du

Received: 16 June 2013 / Accepted: 10 March 2014 / Published online: 28 March 2014

Abstract Polishing is usually indispensable process when better surface roughness is required for the parts such as injection mold. However, polishing process is often performed by manual operations. In this paper, an automatic polishing method for the metal parts with curved surfaces is proposed based on a machining centre. In order to realize the control of contact force, the relationship between the displacement of polishing disk and the force impacted on the polished part is first established. Then, within the contact zone between the polishing disk and the polished part, a pressure distribution model is derived for planar and curved surface polishing according to the specific process parameters. On this basis, the model of removal depth distribution along the vertical direction of feed is built for each polishing pass, and thus a suitable stepover size is further obtained so as to reduce the fluctuations of remove depth to most extent. Finally, an effective planning algorithm of cutter location data in polishing is proposed for a given CNC machine tools, and validation experiments are performed on planar and curved parts. The results show that the proposed automatic polishing scheme is able of achieving a mirror effect surface and keep a good global uniformity, at the same time it improves the polishing efficiency and realizes the integration with milling process.

Keywords Automatic polishing · Curved surface · NC machining · Removal rate · Pressure distribution

D. Feng · Y. Sun (✉) · H. Du
Key Laboratory for Precision and Non-Traditional Machining Technology of the Ministry of Education, Dalian University of Technology, Dalian 116024, China
e-mail: xiands@dlut.edu.cn

1 Introduction

Currently, the requirements of the industry for high quality precision parts with complex geometries have become higher [1–5]. The final surface finishes of some metal parts such as molds are usually implemented by polishing operations in order to reduce the surface roughness of the machined part. However, the polishing process after numerical control (NC) milling of these parts mainly depends on manual operations. It not only is time-consuming and easily producing severe dependence on the worker's experience, but also is difficult to maintain a stable polishing operation for a long time. Therefore, no matter from the perspective of productivity, cost, or the stability of product quality, automatic polishing process is highly desirable due to the advantages of robot or machining centre in force and trajectory control.

The construction of automatic polishing system is mainly based on industrial robot platform [6–11]. For example, Tsai [6–8] developed an AMPS platform which integrates mold geometry process kernel, path planner, process planner, and force control robot into the system. On the other hand, some researchers conducted the automatic polishing on machining centres or grinding machines [12–14] to realize the integrated production from milling or grinding to polishing process. Generally, robot arm-based polishing often uses an active end-effector while the machining centre-based polishing usually uses a passive tool due to the difference of position accuracy of two types of polishing platform. According to the validation results, both two types of polishing patterns can achieve similar finished surface since their fundamental polishing mechanisms are the same for the specific parts. Once the polishing platform is built, the remaining task is to develop the systematic techniques for some concrete materials and parts.

The polishing of curved surface is very complicated and many factors can affect the final polishing results. For

example, Tam [15] investigated the effects of different tool paths on the removal of material in polishing. Rososhansky and Fengfeng [16] proposed the coverage based tool-path planning. They plan the polishing path use the Contact Area Map (CAM) to ensure a complete coverage for polishing. In the study of Huisson et al. [17], the effects of various parameters on the resulting surface are researched for polishing die with a flexible abrasive disk. Zhang [18] investigated the material removal in polishing with fixed abrasives. Lin [19] proposed a path-planning method using an industrial robot. Xi et al. [20–22] developed a complete robotic polishing/deburring system that consists of a hybrid robot and a dual-purpose compliant tool head, and a model of contact stress between the polishing tool and the part is established for an automated polishing process. Then, the experiment results demonstrate the effectiveness of the methods.

As above mentioned, during polishing processes, maintaining a uniform removal depth is very important for precision surface polishing. However, investigations on the model of material removal depth are limited in the existing references for different polishing patterns and polishing tools. In this paper, systematic techniques are developed for the automatic precision polishing of curved surface on a five-axis machining centre with an elastic polishing disk. A pressure distribution model is first derived and validated. Then, a removal depth model is subsequently built and testified. Following, the stepover size determination and cutter location planning strategy for uniform material removal depth are given. Finally, the experimental results are reported in which the proposed polishing method has ability of achieving a precision finish surface with mirror effect.

2 Pressure distribution model

As shown in Fig. 1, an elastic disk is mounted on the spindle of a five-axis machining centre to conduct the polishing operation. Compared with the elastic polishing disk, the milled metal part can be regarded as rigid. Therefore, only the elastic deformation of polishing disk is considered in calculating the contact pressure between the polishing disk and part. In Fig. 1, point A is the critical point between the undeformed region and deformed region of polishing disk on the plane constructed by the tool axis direction and feed direction. Vector $\boldsymbol{n}$ represents the unit surface normal vector at point A, and $\boldsymbol{u}$ represents tool axis direction. θ is the angle between $\boldsymbol{u}$ and $\boldsymbol{n}$ direction. When the elastic polishing disk contacting the part with a given pressure, it will generate contact deformation due to the elastic deformation of the polishing disk. From Fig. 1, it can be seen that the tool displacement E has relationships with the cutter diameter and the tilt angle of cutter. When polishing a metal part using a given polishing disk with a fixed tilt angle, the contact

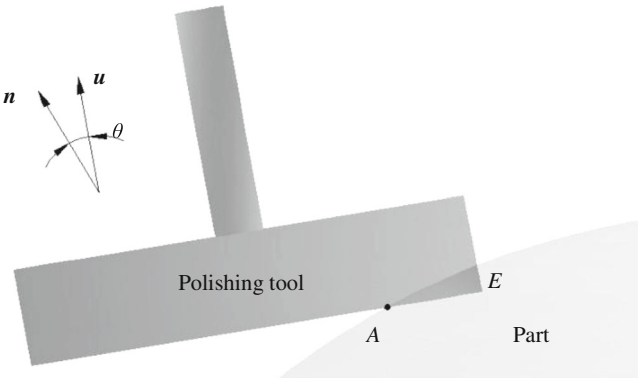

Fig. 1 The position of the part and polishing tool

pressure p at an arbitrary point within the contact zone is proportional to the amount of deformation e in this point and the relation function is assumed as follows:

$$p = k(E)e \tag{1}$$

where $k(E)$ is a coefficient related to the tool displacement E and the polishing status. In this section, the pressure distribution model is derived on the planar firstly, and then it is expanded to the free-form surface.

2.1 Polishing force

For establishing the pressure distribution model in polishing, the relations between the contact force F and tool displacement E should be obtained first. Therefore, a pressure experiment is curried out and the polishing forces corresponding to some given tool displacements are measured with a MINI45 force sensor produced by ATI company. In the experiments, a rubber-polishing disk with 120-mm diameter and a sponge disk with 100-mm diameter are used, and three different tilt angles (5°, 10°, and 15°) are chosen to carry out the experiment. The shaft of polishing disk is first connected with the force sensor and the other end of the sensor is mounted on the spindle of the machine.

When the polishing disk contacts with the part with a minimal contact force, at the moment the displacement of polishing disk is given as 0 and the position is viewed as the initial position of contact. Then, under the condition of keeping a fixed tilt angle of polishing disk, gradually increase the tool displacement with a uniform interval 0.1 mm, and the corresponding values of contact force are sequent measured and recorded. After that, the axial components of these measured forces can be used to build the analytic relations between the tool displacement and contact force.

According to the variation trend of contact force with respect to an increasing tool displacement, a quadratic

polynomial about tool displacement is used to express the contact force.

$$F(E) = aE^2 + bE + c \tag{2}$$

where a, b, and c are the unknown variables which need to be determined according to the measured data of contact force. To fit the measured value, a least square method is used and the coefficients a, b, and c can be obtained by solving the following equations:

$$\begin{pmatrix} (g_1,g_1) & (g_2,g_1) & (g_3,g_1) \\ (g_1,g_2) & (g_2,g_2) & (g_3,g_2) \\ (g_1,g_3) & (g_2,g_3) & (g_2,g_3) \end{pmatrix} \begin{pmatrix} a \\ b \\ c \end{pmatrix} = \begin{pmatrix} (f,g_1) \\ (f,g_2) \\ (f,g_3) \end{pmatrix} \tag{3}$$

where

$$\left(g_k, g_j\right) = \sum_{i=1}^{3} g_k(E_i) g_j(E_i)$$

$$\left(f, g_j\right) = \sum_{i=1}^{3} F_i g_j(E_i) \quad g_1 = E^2, \quad g_2 = E, \quad g_3 = 1$$

For the given polishing disk and corresponding tilt angles, the values of coefficients a, b, and c are calculated and summarized in Table 1. The measured contact forces and fitting curves are illustrated in Fig. 2. The fitting results show that the coefficient of determination R^2 were greater than 99 % for each case and indicates that the regression curves have good agreement with the experimental values.

2.2 Contact pressure on the plane

In planar polishing, the contact zone between the polishing disk and the machined part can be easily determined for a fixed tool displacement E. Theoretically, it is the region enclosed by a chord segment and a circular segment. To obtain the contract pressure, a contact model for the tilting polishing tool is proposed. As illustrated in Fig. 3, taking the critical point A as an original point, then a local coordinate system xAy can be established. The x-axis is along the feed direction of tool and the y-axis is perpendicular to the feed direction of tool on the contact plane. The tilt angle of the polishing disk with respect to the vertical direction of contact plane is set as θ, and the radius value of polishing disk is R. At contact line BC, namely the transition position from undeformed region to the deformed region, the contact pressure can be viewed as 0. However, the contact pressure at point G is up to maximum value since a maximum deformation occurred at the contact position. From this point, a linear distribution of pressure along x-axis direction is assumed to construct the pressure distribution model.

Table 1 The valves of coefficients

Tilt angle		5°	10°	15°
Rubber disk	a	0.594	0.815	0.501
	b	8.493	3.378	2.394
	c	0.087	−0.031	0.043
Sponge disk	a	0.271	0.086	0.053
	b	0.264	0.426	0.212
	c	−0.007	−0.021	0.011

As shown in Fig. 3, along x-axis direction let the length from the origin to the outward edge of polishing disk edge be L, and then L is calculated as

$$L = E/\tan\theta \tag{4}$$

The pressure distribution along x-axis direction is a linear function of variable e, and then we have

$$p(x) = k(E)e = k(E)\tan\theta x \tag{5}$$

where e represents the amount of deformation at a point within the contact zone; $k(E)$ represents the proportion coefficient and it will vary with the change of tilt angle and displacement E of the given polishing disk.

Meantime, the compression deformation along y-axis direction keeps constant in plane polishing process. For example, at the critical contact position BC ($x=0$) between the part and polishing disk, the pressure values along the line are all 0.

Therefore, let $k_\theta(E)=k(E)\tan\theta$, then the pressure within the contact zone in planar polishing can be defined as follows:

$$p(x,y) = k_\theta(E)x \tag{6}$$

Further, the contact force $F(E)$ is given as

$$F(E) = \iint_S p(x,y)dS = \int_{-y\_\max}^{y\_\max} dy \int_0^{f(y)} p(x,y)dx \tag{7}$$

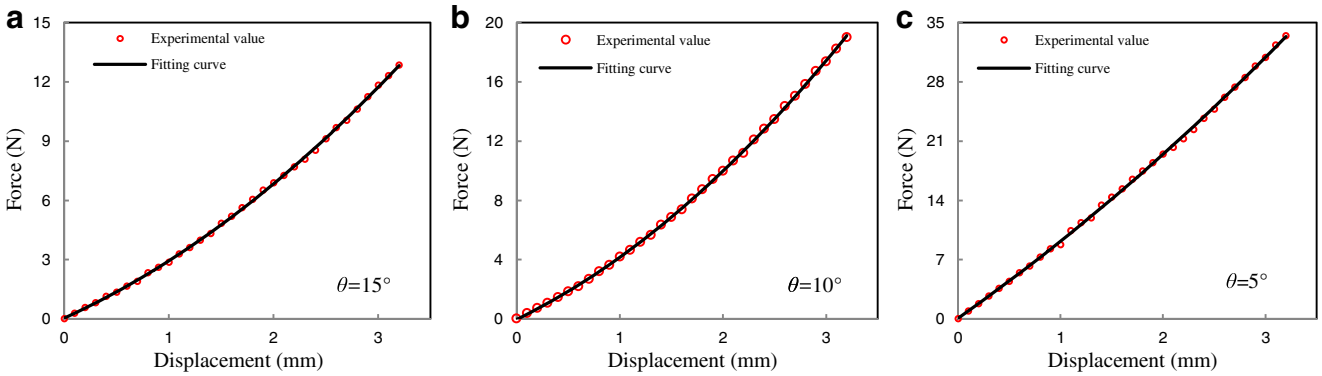

Fig. 2 Relationship between the experiment value and fitting curve of rubber disk

where y_max denotes the half-width of the contact zone, and $f(y)$ is the boundary of the contact zone, they can be expressed, respectively, as

$$y\_\max = \sqrt{R^2-(R-L)^2}, \quad f(y) = \sqrt{R^2-y^2}-R+L$$

According to Eq. (7), the coefficient $k_\theta(E)$ can be described as

$$k_\theta(E) = \frac{2F(E)}{\int_{-y\_\max}^{y\_\max} f(y)^2 dy} \tag{8}$$

Thus, according to the given tool displacement E in polishing, the polishing force can be derived using Eq. (2), then from Eq. (8) the proportional coefficient $k_\theta(E)$ is calculated and the final pressure distribution in planar polishing can be obtained using Eq. (6). Figure 4 shows the pressure distribution within the contact zone in planar polishing with a 120-mm diameter rubber disk. The related parameters are E= 1.0 mm, θ=10°, and $k_\theta(E)$=0.0092.

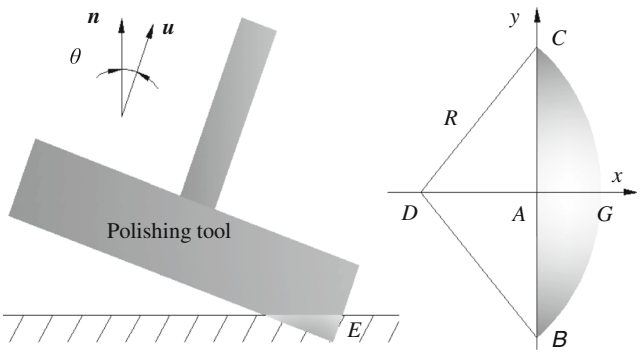

Fig. 3 The contact zone on the plane

2.3 Contact pressure on the curved surface

Using the same way, the pressure distribution model on the regular curved surface such as spherical surface or cylindrical surface can be built. For a given polishing force, in calculating the contact pressure distribution the most important step is to get the compression deformation e of a point within the contact zone. As illustrated in Fig. 5, without losing generality, the machined surface is described as a Bspline surface $\boldsymbol{s}(u,v)$. The bottom plane of the polishing disk is intersected with the surface at BC, where BC represents the critical position from unreformed region to the deformed region of the given polishing disk. Similarly to the case of planar polishing, the contact pressure at the critical position can be viewed as 0.

As shown in Fig. 5, point P is an arbitrary point on the bottom plane of the polishing disk. $\boldsymbol{u}$ is a unit vector which represents the tool axis direction. A straight line, which is parallel to the $\boldsymbol{u}$ direction and through point P, intersects with the free-form surface in point Q. If $(\boldsymbol{Q}-\boldsymbol{P})\cdot\boldsymbol{u}>0$, P is below the machined surface. In this case, it means the polishing disk has contacted the machined surface and generated an elastic deformation amount PQ. Else if $(\boldsymbol{Q}-\boldsymbol{P})\cdot\boldsymbol{u}>0$, it means point P

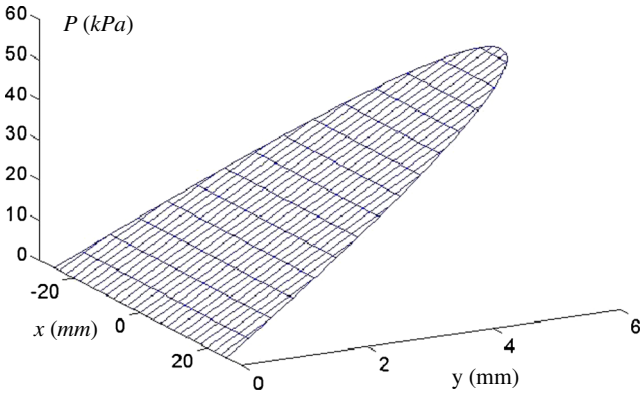

Fig. 4 The pressure distribution in contact zone

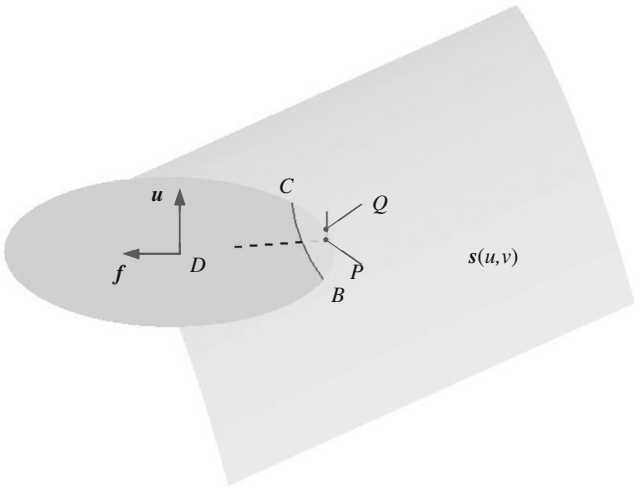

Fig. 5 Contact form on free surface

is above the machined surface and the polishing disk does not contact the machined surface at the position.

Given a point P on the bottom place of a polishing disk, the line parallel to the $\boldsymbol{u}$ direction and through point P can be described as

$$\boldsymbol{L}(e) = \boldsymbol{P} + e\boldsymbol{u} \tag{9}$$

where e is a variable. Thus, the intersection point Q between the line $\boldsymbol{L}(e)$, and the machined surface $\boldsymbol{s}(u,v)$ can be derived from the following equation:

$$\boldsymbol{P} + e\boldsymbol{u} = \boldsymbol{s}(u,v) \tag{10}$$

Eq. (10) is a vector form and thus provides three individual component equations. Therefore, three unknown variables u, v, and e can be obtained from the above equations by using a quasi-Newton method.According to Eq. (10), a function $\boldsymbol{R}(u,v,e)$ can be defined as follows:

$$\boldsymbol{R}(u,v,e) = \begin{cases} r_1(u,v,e) = Q_x(u,v) - P_x - eu_x \\ r_2(u,v,e) = Q_y(u,v) - P_y - eu_y \\ r_3(u,v,e) = Q_z(u,v) - P_z - eu_z \end{cases} \tag{11}$$

where $\boldsymbol{R}(u,v,e)$ is a ternary system of nonlinear equations. Then, a quasi-Newton method can be used to solve the Equation $\boldsymbol{R}(u,v,e)=0$, and the iteration relations are described as

$$\begin{cases} \boldsymbol{w}_{k+1} = \boldsymbol{w}_k - C_k^{-1}\boldsymbol{R}(\boldsymbol{w}_k) \\ C_{k+1} = C_k + \dfrac{(\boldsymbol{t}_k - C_k\boldsymbol{s}_k)(\boldsymbol{s}_k)^T}{(\boldsymbol{s}_k)^T\boldsymbol{s}_k} \end{cases} \tag{12}$$

where

$$\boldsymbol{w}_k = (u_k, v_k, e_k)^T \quad \boldsymbol{s}_k = \boldsymbol{w}_{k+1} - \boldsymbol{w}_k$$
$$\boldsymbol{t}_k = \boldsymbol{R}(\boldsymbol{w}_{k+1}) - \boldsymbol{R}(\boldsymbol{w}_k)$$

When $k=0$, $\boldsymbol{w}_0=(u_0,v_0,e_0)^T$ is the initial value of the iteration process. u_0 and v_0 are the same as the parameters of the cutter contact (CC) point A, and e_0 is usually set as 0. Then the initial matrix C_0 is described as follows

$$C_0 = \begin{pmatrix} \partial r_1/\partial u & \partial r_1/\partial v & \partial r_1/\partial e \\ \partial r_2/\partial u & \partial r_2/\partial v & \partial r_2/\partial e \\ \partial r_3/\partial u & \partial r_3/\partial v & \partial r_3/\partial e \end{pmatrix}_0$$

Setting the termination conditions by $\boldsymbol{s}_k$, when $\boldsymbol{s}_k$ meets the termination conditions, the iteration will be finished. Then, the value of e can be obtained.Thus, using the given algorithm a series of position point on the critical curve BC can be obtained and therefore the contact zone is subsequently determined. Further, if an arbitrary given point P is within the contact zone, and then the deformation amount e at this point can be calculated by Eq. (10). And finally, the total force impacted on the contact zone can be built

$$F = \iint_S k(E)e\,dS \tag{13}$$

where F represents the polishing force. Further, the coefficient $k(E)$ can be described as

$$k(E) = \frac{F}{\iint_S e\,dS} \tag{14}$$

where S represents the contact zone. Therefore, once the coefficient $k(E)$ is obtained, the pressure distribution at each point within the contact zone can be described as

$$p = k(E)e \tag{15}$$

3 Material removal profile

The removal profile in polishing describes the distribution of removal depth along the direction perpendicular to the tool path [18]. It plays an important role in controlling the material removal rate and determining the stopover size. When

polishing with a tilting polishing disk, the deformation amount at each point within the contact zone is variable, so the removal depth perpendicular to the feed direction is unable to keep constant in one pass. Hence, in order to acquire a uniform removal depth, it is necessary to allow the overlap of polishing area when planning two adjacent tool paths. That is to say, the same area may be covered more than once in one step.

3.1 Removal depth distribution

Since the contact zone only occupies a small proportion relative to the overall polishing disk, it is assumed that the sliding velocity due to the rotation of the spindle is the same within the contact zone. In actual polishing, the linear velocity due to rotation of the spindle is far greater than the feed speed. So, ignore the feed speed, and then the sliding velocity within contact zone can be expressed as

$$v_s = \frac{1}{2} \times 2\pi n(R_1 + R_2) = \pi n(2R-L) \tag{16}$$

where n is the speed of spindle. R_1 and R_2 are the max and min radii of the contact zone. L is the difference between the two radius values, which is defined as contact length.

As seen in Fig. 6, the contact zone between the polishing disk and the metal part is a part of circle. The feed motion of polishing disk is at the speed of v_f. Taking a point A on the critical position as the original point, a coordinate system xAy in the bottom plane of the polishing tool is also built. After determining the critical position BAC and the circular segment BGC, the pressure at an arbitrary point M within the contact zone can be obtained by Eq. (15).

According to the theory of Zhang [18], the removal depth value at point M can be expressed as

$$dh = \frac{k_1 F_0 s}{H_V dxdy} = \frac{k_1 p v_s}{v_f H_V} dl \tag{17}$$

where k_1 is a dimensionless coefficient associated with machining system; H_V is the material hardness; v_s represents the sliding speed at the point; v_f is the projection of the feed speed of the polishing tool. Substitution of Eq. (15), (16) into Eq. (17) gives

$$dh = A\frac{n}{v_f}(2R-L)k(E)edl \tag{18}$$

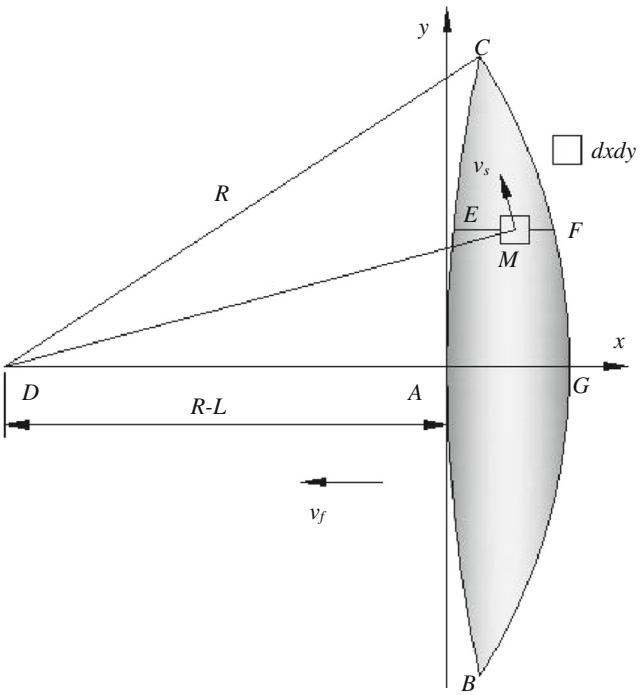

Fig. 6 The contact zone

where $A=k_1\pi/H_V$, is a special coefficient which combines the effect of k_1, and the hardness of the metal part; e is the deformation amount of the polishing disk at different contact point.

The removal distribution perpendicular to the feed direction is obtained by integrating the Eq. (18), then

$$h(y) = A\frac{n}{v_f}(2R-L)\int_{y\_start}^{y\_end} k(E)edx \tag{19}$$

where y_start and y_end are the coordinate values at different y locations such as point E and F in Fig. 6. For calculating Eq. (19), the following approximation method can be used

$$h(y) = A\frac{n}{v_f}(2R-L)\frac{y\_end-y\_start}{N}\sum_{1}^{N} k(E)e \tag{20}$$

where N is the number of the discrete points. Thus, the removal depth distribution can be obtained. For the case of planar polishing, the value of y_start and y_end are expressed as

$$y\_start = 0, \quad y\_end = \sqrt{R^2-y^2}-R+L$$

So, in planar polishing the removal depth distribution may be simplified as

$$h(y) = Ak_\theta(e)\frac{n}{2v_f}(2R-L)\left(\sqrt{R^2-y^2}-R+L\right)^2 \quad (21)$$

From Eq. (21), it can be seen that the removal depth is proportional to the spindle speed n, and inversely proportional to the feed rate v_f.

3.2 Removal profile experiment

An experiment is performed to evaluate the model of calculating material removal profile. A planar block of mold steel NAK80 is polished with a rubber disk pasted by a sand paper. The experimental parameters are shown in Table 2. The removal profile corresponding to 80# Al_2O_3 abrasive is measured, respectively, by contour gauge (Prismo navigator produced by Carl Zeiss AG). According to the measured value, the coefficient A is derived and the results associated with 80 grade abrasive are 0.2911 under the process parameters listed in Table 2. The experimental and theoretical removal profiles are illustrated in Fig. 7. The results show that the removal profile values predicted by the established theoretical model have a good agreement with the experimental values.

3.3 Stepover size determination

The polishing process includes two steps, namely pre-polishing and final-polishing. Pre-polishing is performed after the milling process to eliminate tool marks. In addition, the uniform removal of machined surface in pre-polishing is also crucial for maintaining the profile accuracy and reducing the waviness of the finished surface to most extent. However, due to the uniformity of pressure distribution, the removal depth perpendicular to the feed direction is different. Therefore, an effective control strategy of uniform removal must be considered in planning two adjacent paths. One of main parameters used to keep the uniform removal in polishing is the stepover size.

Equation (20) describes the removal depth formed by one-pass polishing. When an area is polished by multi-pass paths, the removal depth of this area is calculated by

$$H(y) = h(y) + \sum_{i=1}^{n} h(y + iM_d) \quad (22)$$

where M_d is the stepover size. To keep the uniform removal during the polishing process, one solution is to try to maintain a constant removal depth through making the polishing domains of two adjacent tool paths generate suitable overlap. For example, as shown in Fig. 8, in planar polishing if the removal depth at $y=0$ location is half of the maximum value $H_{\max}$ of removal depth, such an overlap between two adjacent tool paths can lead to generate a removal peak at the middle position of stepsize. And, it is an effective means to reduce the fluctuation of remove depths. Let $h(y_d)=h(0)/2$, then the following equation can be obtained

Table 2 The parameters of test

Diameter	Spindle speed	Feed speed	Displacement
120 mm	1,500 r/min	5 mm/s	1.0 mm

$$\left(\sqrt{R^2-y_d^2}-R+L\right)^2 = \frac{1}{2}L^2 \quad (23)$$

Through Eq. (23), the position coordinate y_d can be further derived

$$y_d = \sqrt{R^2-\frac{\left(L+\sqrt{2}(R-L)\right)^2}{2}} \quad (24)$$

Thus, in this case, the stepover size between two adjacent tool paths can be selected as twice as y_d. Generally, for the case of polishing a large mold surface with a small polishing disk, the curvature effect of the surface at local contact zone is usually negligible and the stepover size determination method in planar polishing can be directly utilized.

4 Cutter location planning

Cutter location planning is crucial to improve the machining efficiency and ensure the quality of the products. In planning tool paths, an initial path is first constructed in the parameter or planar domain. Correspondingly, the real tool contact point path is obtained in physics space [23, 24]. Then according to the stepover size derived from computation, the unidirectional contact trajectories are sequent implemented both in parameter space and physical space. For the given contact length L and tilt angle of polishing disk, the tool contact point (CC) paths can be converted into cutter location (CL) point paths. Finally, the CL data also needs to be transformed to machine control data based on the concrete machine configuration.

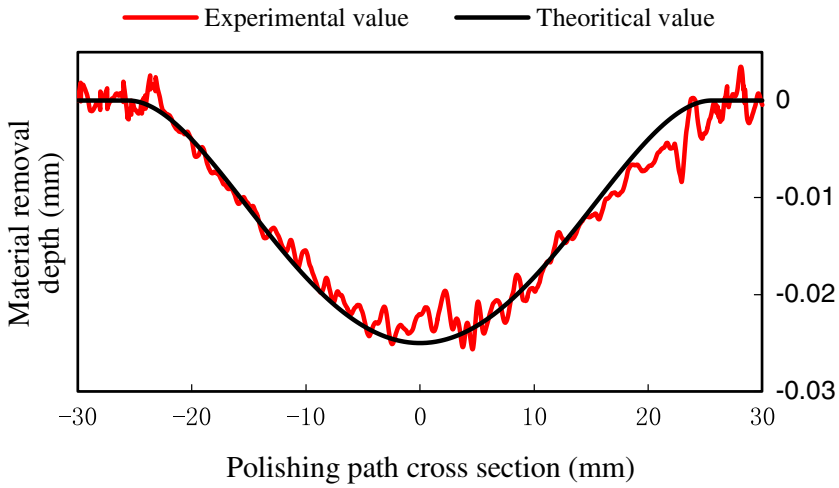

Fig. 7 The removal profile

4.1 Parametric increment calculation

Free-form surface in manufacturing is often expressed as parametric Bspline surface $\boldsymbol{s}(u,v)$, and thus the two parameters u and v of the surface is usually defined in parametric range [0, 1]. For a given tool path, the path interval and its corresponding parametric increment will be obtained first to determine the next path. As illustrated in Fig. 9, P_{i-1} and P_i are two adjacent tool paths and $P_{i-1,j}$ is a point on the tool path, according to the given stepover size, the $P_{i,j}$ corresponding point $P_{i-1,j}$ on the path P_{i} will satisfy the following equation:

$$\frac{\partial \mathbf{s}(u,v)}{\partial v}\Delta v + \frac{\partial \mathbf{s}(u,v)}{\partial u}\Delta u = M_d \boldsymbol{b} \tag{25}$$

where $\boldsymbol{s}(u,v)$ is the equation of free-form surface, and M_d is the stepover size between the adjacent paths. $\boldsymbol{b}$ is a unit vector tangential to the surface and is defined as

$$\boldsymbol{b} = \boldsymbol{n} \times \boldsymbol{f} \tag{26}$$

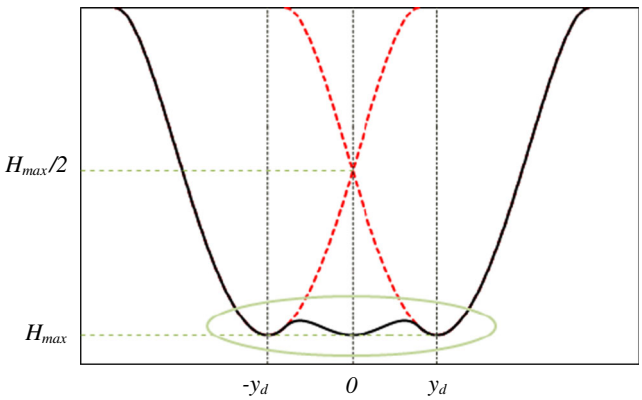

Fig. 8 The superposition of removal depth

where $\boldsymbol{n}$ denotes the unit normal vector at point $P_{i-1,j}$ of the surface. $\boldsymbol{f}$ denotes the unit vector in the direction cutter feed, which can be obtained by the derivation of P_{i-1} path in the actual surface.

From Eq. (25), it can be seen that the parametric increment $\Delta c=[\Delta u,\Delta v]$ at point $P_{i-1,j}$ should be obtained in order to the point $P_{i,j}$ on the P_i path. Eq. (25) is in a vector form and provides three individual component equations. Among them, one component depends on the others, so only two axial components of the equation are needed to calculate the parametric increment Δu and Δv.

$$\begin{pmatrix} \frac{\partial X}{\partial u} & \frac{\partial X}{\partial v} \\ \frac{\partial Y}{\partial u} & \frac{\partial Y}{\partial v} \end{pmatrix} \begin{pmatrix} \Delta u \\ \Delta v \end{pmatrix} = M_d \begin{pmatrix} b_X \\ b_Y \end{pmatrix} \tag{27}$$

By solving Eq. (27), the parameter increment Δu and Δv are described as

$$\Delta u = \frac{M_d \begin{vmatrix} b_x & X_v \\ b_y & Y_v \end{vmatrix}}{\begin{vmatrix} X_u & X_v \\ Y_u & Y_v \end{vmatrix}}, \quad \Delta v = \frac{M_d \begin{vmatrix} b_x & X_u \\ b_y & Y_u \end{vmatrix}}{\begin{vmatrix} X_v & X_u \\ Y_v & Y_u \end{vmatrix}} \tag{28}$$

where X_u is X/u; X_v is X/v. In the same way, Y_u is Y/u; Y_v is Y/v. Then, the parametric coordinate of point $P_{i,j}(u_i,v_i)$ can be written as

$$\begin{pmatrix} u_i \\ v_i \end{pmatrix} = \begin{pmatrix} u_{i-1} \\ v_{i-1} \end{pmatrix} + \begin{pmatrix} \Delta u \\ \Delta v \end{pmatrix} \tag{29}$$

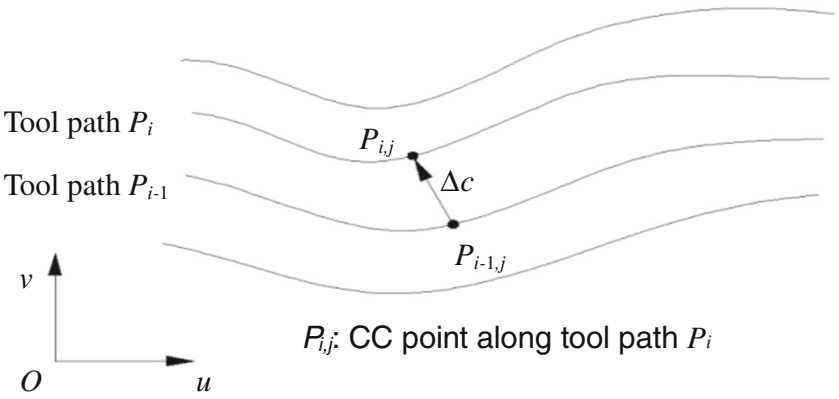

Fig. 9 Construction of the *u-v* curves in parametric domain

When all location points of tool paths are implemented using the above planning strategy, the operation of generating tool contact point path is finished. Specially, when constructing uniform contact paths, we should pay more attentions to the following issues:

1. Theoretically, the initial contact path can be selected at any position of the surface. An initial path that is helpful to reduce the geometric complexity of paths is more desirable.
2. In determining corresponding point of adjacent path, if $u+\Delta u$ or $v+\Delta v$ exceed their parameter ranges, the point should be neglected.
3. With the consideration of removal uniformity, the paths of different polishing steps had better not coincide with each other and keep suitable spacing.

4.2 Cutter location point generation

To polish a given part on a five-axis machining centre with a polishing disk, although it is different from conventional milling with a ball-end or flat-end cutter, it also faces the problem of converting CC points to the CL points. Generally, in the existing CAM software, there are no tool path-planning modules for polishing, so a path-planning algorithm is proposed here for surface polishing with a tilting-polishing disk. According to the given CC point paths and the machined surface, the position coordinates of each CC point and the unit normal vector at this point of the surface can be derived. Then, these CC points and their associated surface normal vector can be used to generate CL data. Once the machine configuration is given, NC codes can be generated from these CL data to control the machine to perform the polishing task.

The position relation between the CL point and the CC point in polishing is shown in Fig. 10. Point A is a CC point and it has a distance L from the outward edge of the polishing disk, where L can be obtained by the Eq. (4). Point D is the CL point corresponding to the CC point A. It is the central position of the bottom plane of polishing disk. The CL data consists of the tool axis vector $\boldsymbol{u}$ and space location vector $\boldsymbol{D}$. Vectors $\boldsymbol{A}$ and $\boldsymbol{n}$, respectively, represent the space position of the CC point and the unit normal vector at the point of the machined surface. $\boldsymbol{f}$ is a unit vector along the feed direction.

During polishing process, the tool axis vector $\boldsymbol{u}$ lies in the plane formed by vectors $\boldsymbol{n}$ and $\boldsymbol{f}$. Related to the surface normal vector $\boldsymbol{n}$, the main shaft of polishing disk has a fixed tilting angle θ. Then the unit direction vector $\boldsymbol{u}$ of tool axis can be determined with the following expression:

$$\boldsymbol{u} = \frac{\boldsymbol{n}\cos\theta - \boldsymbol{f}\sin\theta}{\|\boldsymbol{n}\cos\theta - \boldsymbol{f}\sin\theta\|} \tag{30}$$

The length L_{AD} of the line segment AD between the CC point A and CL point D can be given as $L_{AD}=R-L$, and the direction vector υ from point A to point D can be calculated using the following formula:

$$\boldsymbol{\upsilon} = \frac{\boldsymbol{f}\cos\theta + \boldsymbol{n}\sin\theta}{\|\boldsymbol{f}\cos\theta + \boldsymbol{n}\sin\theta\|} \tag{31}$$

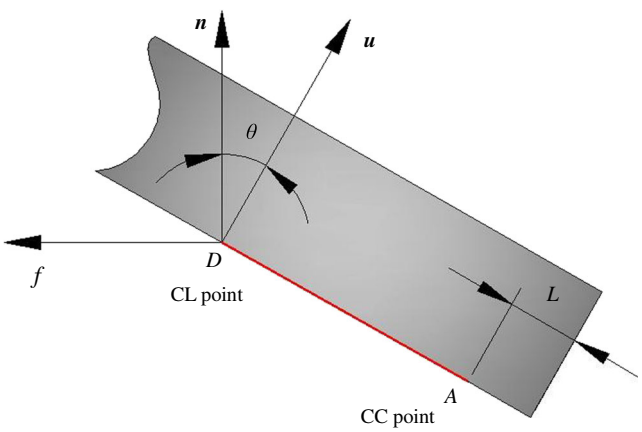

Fig. 10 The tool center point and the cutter contact point

Then the position coordinates $\boldsymbol{D}$ of the CL point D can be given as

$$\boldsymbol{D} = \boldsymbol{A} + (R-L)\boldsymbol{\upsilon} \tag{32}$$

Thus, the position vector $\boldsymbol{D}$ and orientation vector u constitute the CL data $\boldsymbol{C_D}$ at point D corresponding to the CC point A. That is $\boldsymbol{C_D}=(\boldsymbol{D}\ \boldsymbol{u})$.

4.3 Machine tool configuration

The cutter axis vector and the cutter location coordinates mentioned above describe the posture of cutting tool in the workpiece coordinate system. However, it cannot be directly used to drive the machine. The same CL data will be converted to different machine control data due to the difference of machine configurations. Therefore, a necessary post-processing operation will first be performed to generate NC code according to the concrete machine configuration.

In the surface polishing on a five-axis machining centre, a machine with a table/spindle tilting type of configuration is used here. As shown in Fig. 11, coordinate systems, which are necessary for building the kinematic transformation between the cutter's physic locations and the desired machine tool's motions. O_W-$X_WY_WZ_W$ is the work coordinate system (WCS); O_T-$X_TY_TZ_T$ is the tool coordinate system (TCS); O_{m1}-$X_{m1}Y_{m1}$-Z_{m1} is a coordinate system connected to the rotating axis C', and O_{m2}-$X_{m2}Y_{m2}Z_{m2}$ denotes a coordinate system connected to the rotating axis B. In TCS, O_{m2} is defined as $\boldsymbol{r}_{m2}=(0,0,M_2)$, the position vector and axis direction of the cutting tool are defined as (0,0,0) and (0,0,1). In WCS, the position of O_{m1} is defined as $\boldsymbol{r}_{m1}=(m_x,m_y,m_z)$. In order to describe each axis movement quantitatively, the movement of the translational axis is defined as $\boldsymbol{r}_s=(r_x,r_y,r_z)$; the movement of the rotation axis are defined as θ_B and θ_C where the anticlockwise direction is positive.

In the initial status, the spindle direction is parallel to the Z_W direction of WCS. Meanwhile, coordinate system WCS is initially aligned with coordinate system MCS. Then the transformation relationship between the given CL data and the machine control data is described as

$$\begin{cases} (u_x,u_y,u_z,0)^T = T(\boldsymbol{r}_{m1})\cdot R_Z(-\theta_C)\cdot T(\boldsymbol{r}_s-\boldsymbol{r}_{m1}+\boldsymbol{r}_{m2}) \\ \qquad \cdot R_Y(\theta_B)\cdot T(-\boldsymbol{r}_{m2})\cdot(0,0,1,0)^T \\ (D_x,D_y,D_z,0)^T = T(\boldsymbol{r}_{m1})\cdot R_Z(-\theta_C)\cdot T(\boldsymbol{r}_s-\boldsymbol{r}_{m1}+\boldsymbol{r}_{m2}) \\ \qquad \cdot R_Y(\theta_B)\cdot T(-\boldsymbol{r}_{m2})\cdot(0,0,0,1)^T \end{cases} \tag{33}$$

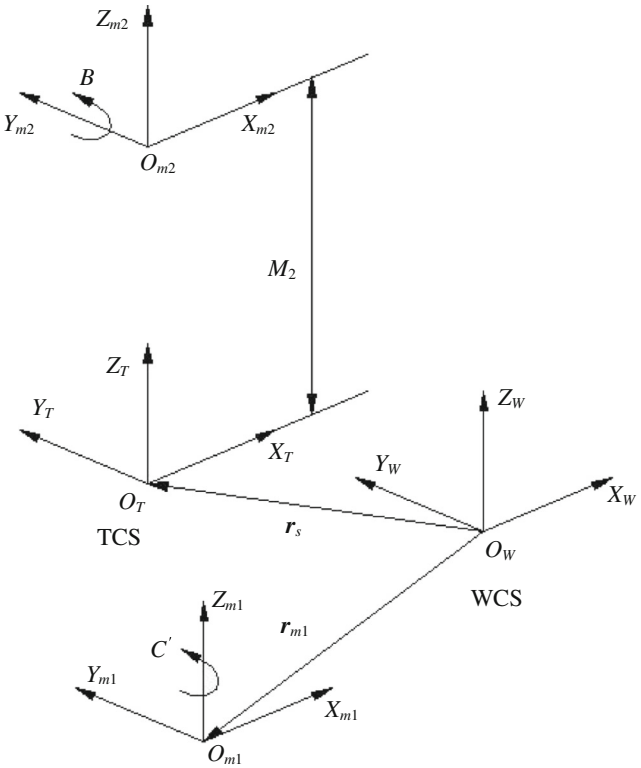

Fig. 11 Machine configuration of C′-B

where

$$T(\boldsymbol{r}_{m1}) = \begin{pmatrix} 1 & 0 & 0 & m_x \\ 0 & 1 & 0 & m_y \\ 0 & 0 & 1 & m_z \\ 0 & 0 & 0 & 1 \end{pmatrix},\ R_Z(-\theta_C) = \begin{pmatrix} \cos\theta_C & \sin\theta_C & 0 & 0 \\ -\sin\theta_C & \cos\theta_C & 0 & 0 \\ 0 & 0 & 1 & 0 \\ 0 & 0 & 0 & 1 \end{pmatrix}$$

$$T(\boldsymbol{r}_s-\boldsymbol{r}_{m1}+\boldsymbol{r}_{m2}) = \begin{pmatrix} 1 & 0 & 0 & s_x-m_x \\ 0 & 1 & 0 & s_y-m_y \\ 0 & 0 & 1 & s_z-m_z-M_2 \\ 0 & 0 & 0 & 1 \end{pmatrix},$$

$$R_Y(\theta_B) = \begin{pmatrix} \cos\theta_B & 0 & \sin\theta_B & 0 \\ 0 & 1 & 0 & 0 \\ -\sin\theta_B & 0 & \cos\theta_B & 0 \\ 0 & 0 & 0 & 1 \end{pmatrix},\ T(-\boldsymbol{r}_{m2}) = \begin{pmatrix} 1 & 0 & 0 & 0 \\ 0 & 1 & 0 & 0 \\ 0 & 0 & 1 & -M_2 \\ 0 & 0 & 0 & 1 \end{pmatrix}$$

Then, the unknown parameters $\boldsymbol{r}_s$, θ_B, and θ_C can be obtained by solving Eq. (33).

5 Experimental verification

In order to validate the proposed approach, polishing experiments are carried out on a DMU60 five-axis machining centre with a table/spindle tilting type of configuration. The tested parts all are made of NAK80 pre-hardened steel. The Rockwell hardness of used material is 42 HRC. Two types of parts, namely planar part and curved part, are used in the

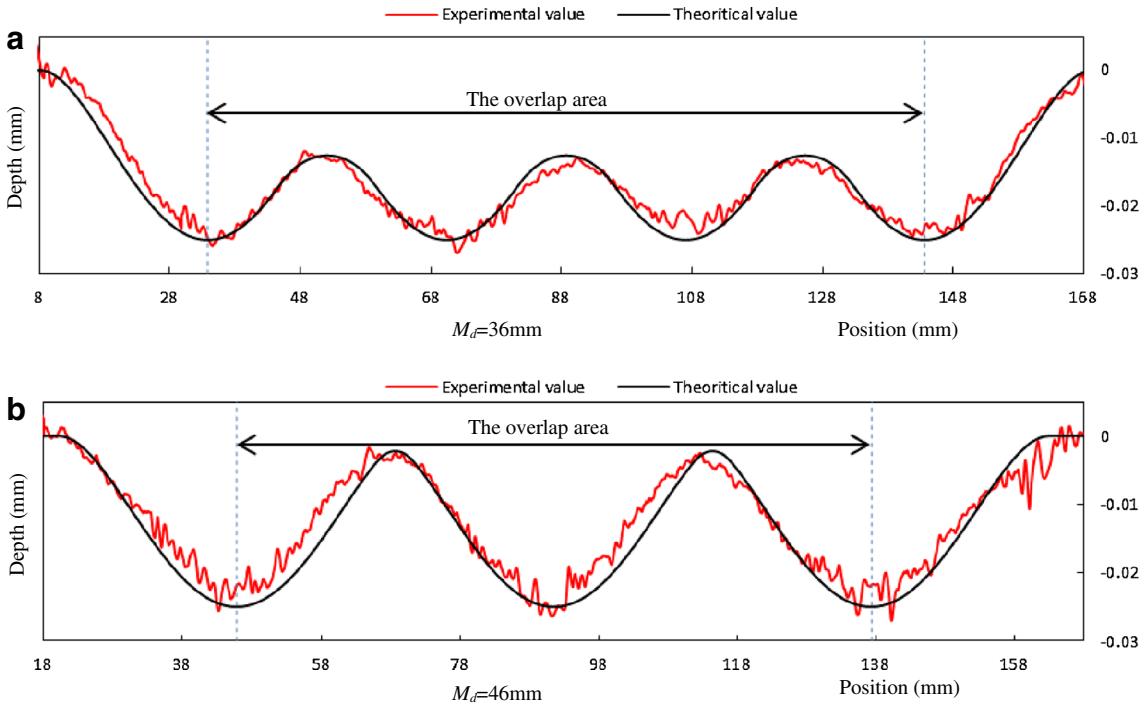

Fig. 12 The removal depth superposition

experiments. The total experiments include two parts: the first is the validation of removal model, where two kinds of path interval on the removal depth profile are conducted in the validation tests. The second is the validation of the polishing results that may be reached using the proposed method. Polishing disk with aluminum oxide (Al_2O_3) abrasives and 120-mm diameter is adhered on the rubber support and used to polishing the workpiece with a 10° tilting angle.

5.1 Validation of removal depth model

Pre-polishing process plays an important role in ensuring the uniform material removal, especially for relatively large particle size of abrasive. For the uniform material removal, the stepover size is an important parameter which needs to be determined. For further confirm the removal depth model on the overlap area, two kinds of stepover size which are 36 and 46 mm are selected to conduct the unidirectional polishing. Two pieces of planar parts with the dimensions of 200 mm × 80 mm × 30 mm are used to conduct the experiment. For the polishing tools, a rubber disk with 80# grade of abrasive is chosen and the machining parameters are illustrated in Table 2. In polishing process, the feed direction is along the width direction of the part. Close to the two boundaries of the part along the length direction, the two marginal areas of the part are kept not removed in experiment in order to be taken as the measuring basis of the follow-up measurement. In the experiment, the surface profile of three positions along the direction of 200-mm length for each part is measured with a contour gauge (Prismo navigator produced by Carl Zeiss AG). Figure 12 describes the removal depth distribution under the

Table 3 Analysis of material removal depth

	M_d (mm)	Expected H_{max}(μm)	H_{ave}(μm)		H_{pro}(μm)	
			Actual	Expected	Actual	Expected
a	36	25	−18.87	−18.91	3.41	4.14
b	46	25	−13.59	−15.15	6.42	6.92

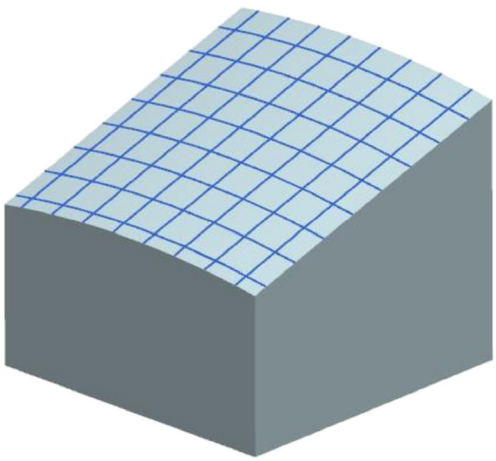

Fig. 13 The curved surface model

Table 4 Process program

Steps	n (rpm)	v_f (mm/s)	M_d (mm)	a_p (mm)	Angle	Time (min)
Milling (Φ12)	1,500	7.5	0.34	0.2	30°	75
Steps	n (rpm)	v_f (mm/s)	M_d (mm)	Angle	E (mm)	Cycle
80 grade	1,500	5	28.2	10°	1.0	6
240 grade	1,500	5	28.2	10°	1.0	6
400 grade	1,500	5	28.2	10°	1.0	6
800 grade	1,500	5	28.2	10°	1.0	6
W2.5 diamond abrasive	1,500	6.7	35.9	10°	2.0	2

condition of polishing with two different stepover sizes. Theoretically, the polishing areas of two adjacent tool paths have some overlap using the given two types of stepover size. Even so, are shown in Table 3, the actual profiles have good agreements with theoretical profiles. Further, for comparing the consistent degree between actual profile and expected one in the superposition area, an evaluation criterion H_{pro}, which reflects the value of fluctuation, is introduced with the following expressions:

$$H_{pro} = \frac{1}{N}\sum_{i=1}^{N} |H(i) - H_{ave}| \tag{34}$$

where

$$H_{ave} = \frac{1}{N}\sum_{i=1}^{N} H(i)$$

where N is the number of measuring point; $H(i)$ represents the removal depth in each point. As can be seen in Table 3, the fact that the actual value is close to the expected value further confirms the correctness of the removal depth model. Meanwhile, the maximum removal depth can be got easily, which is helpful for predict the overall removal depth of polishing process. From the experimental results, it also can be seen that stepover size has an effect on the magnitude of fluctuations of material removal depth. As shown in Fig. 8, such fluctuations can be reduced to the minimum extent by selecting a reasonable stepover size.

5.2 Polishing experiment

In the polishing experiments, a planar part and a curved part are selected with dimensions of 100 mm in length and 100 mm in width. The geometric model of the curved part, whose minimum curvature radius is about 350 mm, is shown in Fig. 13. Before polishing operation, the two parts are both milled with a 12 ball-end cutter. The process parameters in milling and polishing are summarized in Table 4. The cusp height in milling is about 10 μm and the final surface roughness R_a of the two milled parts is about 1.26 μm. For the two milled parts, a rubber disk sticked by 80# sandpaper is first used to remove the tool marks as quickly as possible, then 240#, 600#, and 800# sandpapers are sequent used to reduce the surface roughness gradually. And last, a synthetic diamond paste of grade 2.5 μm is used for the final polishing. In the polishing process with sandpaper, the path interval is calculated using the proposed algorithm with control of uniform removal depth.

Once the two sample parts are polished, the surface roughness of the two parts are measured with a 3D noncontact profilemeter (Newview 5002, Zygo). During planar polishing, corresponding to the 80#, 240#, 400#, and 800# abrasive, the

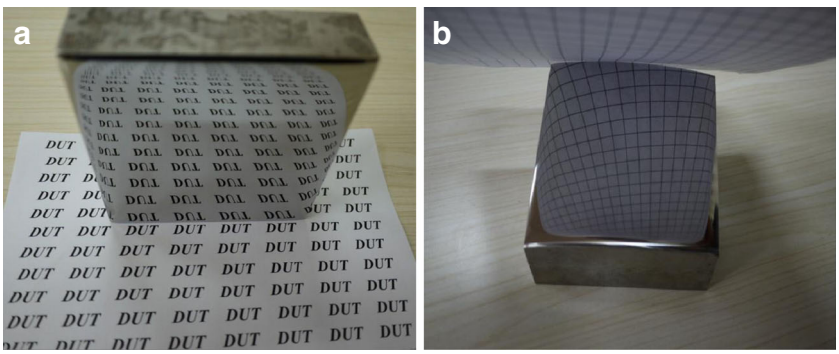

Fig. 14 The final surface

Polished planar part; Polished curved part

final surface roughness of each process step is 0.218, 0.068, 0.042, and 0.023 μm, respectively. After final polishing, the measurement results of planar part and curved part are R_a= 9.077 nm and R_a=17.351 nm, respectively. From the results, it can be seen that the proposed automated polishing method has the ability to reach the degree of mirror finish. The final two polished parts are shown in Fig. 14a and b. The mirror effect of the final polished parts is very obvious. From the reflected images of English characters and crossed meshes, we can see that the two polished surfaces both have good global uniformity of mirror polishing.

6 Conclusion and future work

An automatic precision polishing method for free-form surfaces has been proposed. It is implemented on a machining centre and is helpful for realizing the integration with milling process. Using the proposed polishing model, mirror effect surface are achieved and further validated by the experimental results. In the proposed method, the relation between the polishing force and tool displacement is built using a regress model. It is helpful for realizing the pressure control in polishing surface with a passive tool. For polishing free-form surfaces with a tilting elastic polishing disk, a model of polishing pressure distribution is built within the contact zone of the polished part and the elastic polishing disk. Subsequently, a removal depth model is derived and it is further validated by experimental results. By means of the built removal depth model, suitable stepover size between two adjacent polishing paths is also given to reduce the fluctuations of removal depth to most extent. Then, a cutter location planning algorithm is proposed. The proposed polishing strategy is well tested for the automatic precision polishing of planar and curved parts made of NAK80 mold steel on a machining centre. The validation results show the effectiveness and feasibility of the model as well as its ability to achieve mirror effect surfaces. A further extended work of the model is the realization of specific surface topography.

Acknowledgments This work was supported by the NBRPC (No. 2011CB706800) and NSFC (No. 51321004 and 51075054).

References

1. Hauth S, Linsen L (2012) Cycloids for polishing along double-spiral tool paths in configuration space. Int J Adv Manuf Technol 60(1–4):343–356
2. Shi Y, Zheng D, Liyong H (2012) NC polishing of aspheric surfaces under control of constant pressure using a magnetorheological torque servo. Int J Adv Manuf Technol 58:1061–1073
3. Zhan J (2013) Study on error compensation of machining force in aspheric surfaces polishing by profile-adaptive hybrid movement–force control. Int J Adv Manuf Technol 54:879–885
4. Chen W-C, Kun-Ling W, Yan B-H, Tsao M-C (2013) A study on the magneto-assisted spiral polishing on the inner wall of the bore with magnetic hot melt adhesive particles. Int J Adv Manuf Technol 69: 1791–1801
5. Tian YB, Zhong ZW, Lai ST, Ang YJ (2013) Development of fixed abrasive chemical mechanical polishing process for glass disk substrates. Int J Adv Manuf Technol 68:993–1000
6. Tsai MJ, Huang JF, Kao WL (2009) Robotic polishing of precision molds with uniform material removal control. Int J Mach Tools Manuf 49:885–895
7. Tsai MJ, Chang J-L, Haung J-F (2005) Development of an automatic mold polishing system. IEEE Trans Autom Sci Eng 2:393–397
8. Tsai MJ, Huang JF (2006) Efficient automatic polishing process with a new compliant abrasive tool. Int J Adv Manuf Technol 30:817–827
9. Zhan JM (2013) Study on the manufacturing process controlling for aspheric surface ballonet polishing. Int J Adv Manuf Technol 69: 171–179
10. Tam H-y, Lui OC-h, Mok ACK (1999) Robotic polishing of free-form surfaces using scanning paths. J Mater Process Technol 95:191–200
11. Nagata F, Hase T, Haga Z (2007) CAD/CAM-based position/force controller for a mold polishing robot. Mechatronics 17: 207–216
12. Pessoles X, Tournier C (2009) Automatic polishing process of plastic injection molds on a 5-axis milling center. J Mater Process Technol 209:3665–3673
13. Ahn JH, Lee MC, Jeongetc HD (2002) Intelligently automated polishing for high quality surface formation of sculptured die. J Mater Process Technol 130–131:339–344
14. Ahn JH, Shen YF, Kim HY, Jeong HD, Cho KK (2001) Development of a sensor information integrated expert system for optimizing die polishing. Robot Comput Integr Manuf 17:269–276
15. Tam H-y, Cheng H (2010) An investigation of the effects of the tool path on the removal of material in polishing. J Mater Process Technol 210:807–818
16. Rososhansky M, Xi F (2011) Coverage based tool-path planning for automated polishing using contact mechanics theory. J Manuf Syst 30:144–153
17. Huisson JP, Ismail F, Jafari A, Bedi S (2002) Automated polishing of die steel surfaces. Int J Adv Manuf Technol l19:285–290
18. Zhang L, Tam HY, Yuan C-M, Chen Y-P, Zhou Z-D (2002) An investigation of material removal in polishing with fixed abrasives. Proc Inst Mech Eng B J Eng 216:103–112
19. Lin F-y, Lu T-s (2005) Development of a robot system for complex surfaces polishing based on CL data. Int J Adv Manuf Technol 26: 1132–1137
20. Roswell A, Xi F, Liu G (2006) Modelling and analysis of contact stress for automated polishing. Int J Mach Tools Manuf 46:424–435
21. Xi F, Zhou D (2005) Modeling surface roughness in the stone polishing process. Int J Mach Tools Manuf 45:365–372
22. Liao L, Xi F, Liu K (2008) Modeling and control of automated polishing/deburring process using a dual-purpose compliant tool head. Int J Mach Tools Manuf 48:1454–1463
23. Yuwen S, Dongming G, Zhenyuan J, Haixia W (2006) Iso-parametric tool path generation from triangular meshes for free-form surface machining. Int J Mach Tools Manuf 28:721–726
24. Sun Y, Ren F, Zhu X, Guo D (2012) Contour-parallel offset machining for trimmed surfaces based on conformal mapping with free boundary. Int J Mach Tools Manuf 60:261–271